Measurement of doubly excited levels in lithiumlike and berylliumlike cobalt

A. J. Smith,[1] P. Beiersdorfer,[2] V. Decaux,[2] K. Widmann,[2] A. Osterheld,[2] and M. Chen[2]
[1]*Department of Physics, Morehouse College, Atlanta, Georgia 30314*
[2]*Lawrence Livermore National Laboratory, Livermore, California 94550*
(Received 12 October 1994)

We have measured the dielectronic satellite spectrum for heliumlike Co XXVI trapped and excited in an electron-beam ion trap using a high-resolution x-ray spectrometer in the von Hámos geometry. By sweeping the electron-beam energy across the individual dielectronic recombination resonances, we have determined the relative resonance strengths of the strongest resonances populating doubly excited levels in lithiumlike and berylliumlike cobalt. Most measured dielectronic satellite strengths compare well with theory. A discrepancy with theoretical values is noted for the resonance strength associated with levels $(1s_{1/2}2p_{3/2}^2)_{3/2}$ and $(1s_{1/2}2s_{1/2}2p_{1/2})_{1/2}$. Their values of $49.8\pm3.2\times10^{-20}$ cm^2 eV and $22.9\pm6.4\times10^{-20}$ cm^2 eV, respectively, are almost twice the size predicted by theory.

PACS number(s): 32.30.Rj, 34.80.Kw, 52.25.Nr

I. INTRODUCTION

Dielectronic recombination (DR) is the dominant recombination process in low-density plasmas such as those found in the sun's corona and in tokamak fusion devices. It is a resonance process in which a highly charged ion captures an electron and simultaneously excites a bound electron to an excited state. Such a doubly excited autoionizing state may be stabilized by the emission of a photon (dielectronic recombination); or it may undergo autoionization. In the *KLL* process studied here, a heliumlike ion captures an electron into the *L* shell and excites an electron from the *K* to the *L* shell:

$$1s^2+e\rightarrow 1s2l2l'\rightarrow 1s^22l+h\nu' \ . \tag{1}$$

The stabilizing transitions generate lithiumlike satellites to the heliumlike $K\alpha$ lines. The emitted photon energies $h\nu'$ of the satellite transitions are close to the energies $h\nu$ of the heliumlike transitions

$$1s2l\rightarrow 1s^2+h\nu \ , \tag{2}$$

since the effect of the spectator electron $2l$ is rather small. The DR resonance energy always lies below the energy of the x-ray photon by the $2l$ ionization energy of the lithiumlike charge state. Similarly, recombinations into the lithiumlike ground state with *K*-shell excitation lead to berylliumlike satellites of the heliumlike $K\alpha$ lines. These satellite lines are also of interest in the present study.

High-resolution x-ray measurements on *K* spectra and their associated DR satellite spectra from low-density plasmas provide information on plasma parameters, such as electron temperature, electron density, plasma rotation, and whether or not the electron energy distribution function is Maxwellian [1–8]. In the case of the large tokamaks such as the Tokamak Fusion Test Reactor (TFTR), or the Joint European Torus (JET), studies have concentrated on DR spectra of heliumlike transition metals such as Ti XXI, Cr XXIII, Fe XXV, and Ni XXVII, which often occur as impurity ions in these devices. Studies have also been carried out on the electron-beam ion trap (EBIT) [9,10] at the Lawrence Livermore National Laboratory, where the DR resonances for heliumlike Ni XXVII [11] were mapped, DR satellite transitions in lithiumlike, berylliumlike, and boronlike vanadium were accurately measured [12], and level-specific DR cross sections for Fe XXV [13] were obtained. In the present experiment, we have studied the $K\alpha$ x-ray spectrum of heliumlike Co XXVI and the associated lithiumlike and berylliumlike DR spectra with a high-resolution crystal x-ray spectrometer in the von Hámos geometry. The present measurements were also carried out on the Livermore EBIT. By measuring the excitation function, we have obtained relative resonance strengths of the more prominent DR transitions and compared our results with theory.

II. EXPERIMENT

The measurements were carried out on the Livermore EBIT, in which ions in high-charge states ($\leq 89+$) are ionized, excited, and trapped by an electron beam and studied through measurements of their x-ray emissions. The x-ray photons are recorded by the EBIT von Hámos crystal spectrometer, which has been described elsewhere [14]. In the present experiment, the spectrometer employs a quartz crystal $(20\bar{2}3)$ with a lattice spacing of $2d=2.7947$ Å, bent to a radius $R=120$ cm. The nominal resolving power of this setup is $\lambda/\Delta\lambda=10\,700$ at a Bragg angle of 45° [15], and $\lambda/\Delta\lambda=6200$ at the Bragg angle of 38.71° corresponding to the wavelength of 1.7207 Å, the wavelength of the Cr XXIII resonance line. The wavelength range covered at this setting is 1.71–1.75 Å; this includes the heliumlike transitions of Co XXVI as well as all the lithiumlike and berylliumlike satellites.

In Fig. 1 is shown a spectrum of the heliumlike lines; the resonance line w $(1s2p\ ^1P_1\rightarrow 1s^2\ ^1S_0)$, the intercombination lines x $(1s2p\ ^3P_2\rightarrow 1s^2\ ^1S_0)$, and y $(1s2p\ ^3P_1\rightarrow 1s^2\ ^1S_0)$, and the forbidden line z $(1s2s\ ^3S_0\rightarrow 1s^2\ ^1S_0)$; the lines have been labeled according to a notation by Gabriel [16]. These lines are excited at 6.75 keV, some 100 eV above the threshold for excitation of

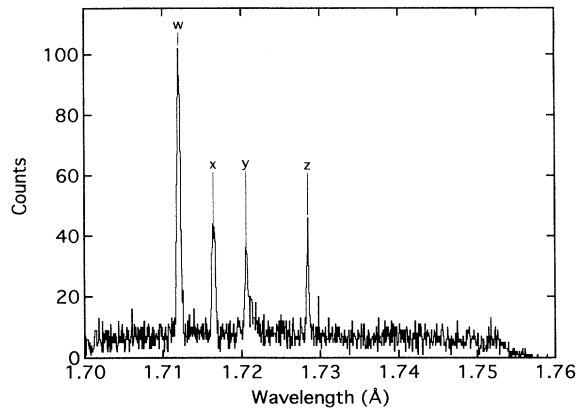

FIG. 1. $K\alpha$ spectrum of heliumlike Co XXVI showing the lines w, x, y, and z. These lines are excited at 100 eV above the energy of the resonance line w. At this energy, no lithiumlike dielectronic satellite lines can be excited; however, the lithiumlike line q can be seen blended with y. q is excited here directly from the lithiumlike state. The cross sections for q and the heliumlike lines are comparable so that the relatively low intensity of q indicates a charge balance in favor of heliumlike states.

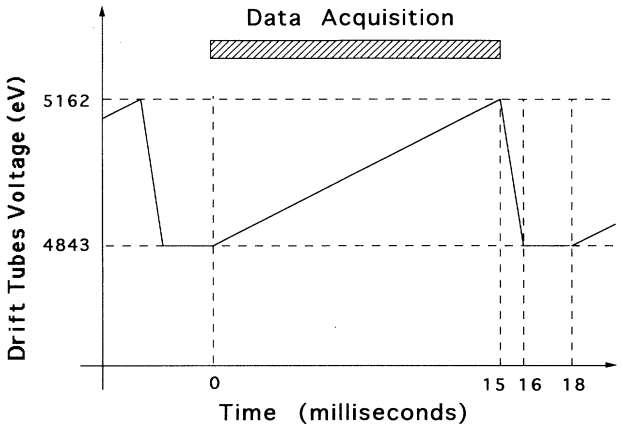

FIG. 2. The electron excitation voltage was swept from 5162 to 4843 eV, a total of 319 eV according to the wave form shown. During the sweep, 15 spectra each of 1-ms duration were stored.

the resonance line w. This energy is far above the KLL dielectronic resonance energies, which lie near 5.0 keV. Thus, no satellite lines contribute to this spectrum and only lines excited directly by electron impact (the so-called direct excitation or DE lines) appear in the spectrum shown in Fig. 1.

Also noticeable in Fig. 1 is the lithiumlike line q ($1s2s2p\ ^2P_{3/2} \rightarrow 1s^2 2s\ ^2S_{1/2}$); the line lies close to and is blended with y. The transition q represents the strongest electric dipole transition of the lithiumlike charge state excited by direct electron impact. (At a different beam energy, the line can also be excited by dielectronic recombination.) The cross section for the excitation of q by direct electron impact is comparable to those of the heliumlike transitions, and the lower intensity of q indicates the charge balance in the trap favors heliumlike states.

We have used the heliumlike lines w, x, y, and z as calibration lines to establish the instrumental dispersion. The transitions have been assigned wavelengths calculated by Drake [17]: $\lambda = 1.712\,00$, $1.716\,42$, $1.720\,59$, and $1.728\,39$ Å for w, x, y, and z, respectively.

To measure the DR line strengths, we have ramped the electron-beam energy through 319 eV according to the wave form shown in Fig. 2. The DR resonance energies for heliumlike cobalt according to the calculations for this paper vary from 4917 eV for the lines o and p to 5069 eV for the line n, an energy spread of 153 eV. We have swept the excitation energy from 5162 to 4843 eV, which more than covers the DR resonances of He-like Co XXVI. In choosing the sweep energies, we took into account space-charge effects, in the amount of 231 eV. Values of the beam energy given throughout this paper refer to the actual electron-ion interaction energies and have been corrected for the space charge of the beam. During the sweep, 15 spectra have been stored, each with a dwell time of 1 ms; the observed spectra are described below.

III. RESULTS

Line identification

In Fig. 3 we show two spectra obtained at two time groups: Figure 3(a) corresponds to an average excitation energy $E = 4983$ eV and Fig. 3(b) to an average excitation energy $E = 5068$ eV. The intensities of the satellite lines excited at the different energies depend on the resonance strength of the line and on the overlap of the resonance with the electron beam. At the lower excitation energy,

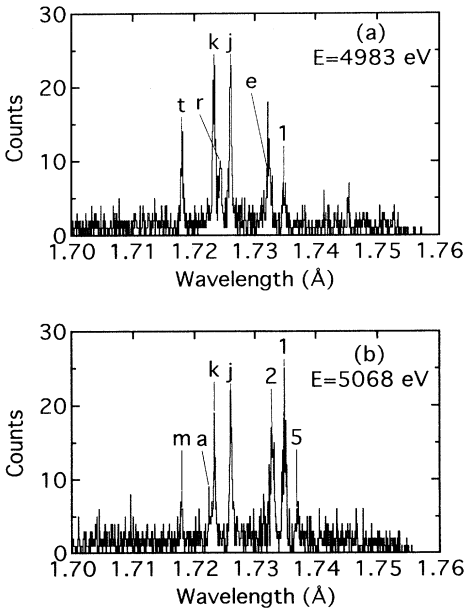

FIG. 3. KLL spectra of Co XXVI, obtained at electron excitation energies (a) 4983 and (b) 5068 eV. The spectra shown indicate that different resonances are sampled at different electron energies. (a) has contributions mostly from satellite lines with lower values of E_{au}, while (b) shows mostly berylliumlike satellites and those with higher values of E_{au}.

the 50-eV spread of the electron beam overlaps the resonances for satellites *r*, *t*, and *e* with resonance energies 4971, 4998, and 5008 eV, respectively. These lines are, therefore, quite prominent in the spectrum shown in Fig. 3(a). The heliumlike line *m*, which is nearly coincident with *t* in wavelength, and the berylliumlike line 2, which is nearly coincident with *e* in wavelength, have resonance energies that are 85 and 100 eV above this excitation energy; therefore, they do not contribute to the spectrum in Fig. 3(a). The higher excitation energy more closely overlaps the resonances for *m* and the berylliumlike satellites; thus, the lines 2, 5, and *m* appear and the line 1 becomes more prominent in the spectrum shown in Fig. 3(b). It should also be noted that the intensity of the line *m* in Fig. 3(b) is about 30% of the intensity of the line *t* in Fig. 3(a); this ratio is consistent with the relative line strengths of these lines (see discussion below). The strong satellites *j* and *k* have resonance energies 5035 and 5026 eV, which lie between the excitation energies shown; thus, they make contributions to both spectra shown.

For comparison with theory, we have added the spectra from time groups 1–15. The sum spectrum is shown in Fig. 4(a). Also shown in Fig. 4 are the theoretical spectra derived from our calculations and from those of Vainshtein and Safronova [19]. These theoretical spectra

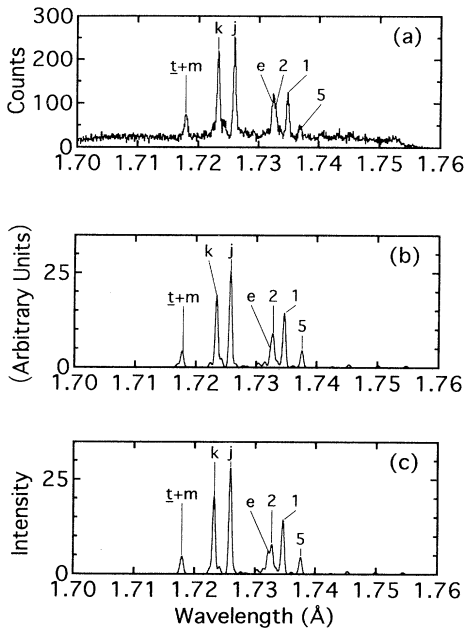

FIG. 4. Dielectronic recombination satellite spectrum for heliumlike cobalt; the experimental spectrum (a) is the sum of the spectra obtained for time groups 1–15. In addition to the more prominent lithiumlike satellites to the $K\alpha$ lines, berylliumlike satellite lines have also been identified. In (b) and (c), theoretical spectra of the dielectronic satellite transitions are shown. These plots, which were generated from atomic-structure calculations for this paper and by Vainshtein and Safronova [19], have been adjusted to include angular distribution and polarization-dependent reflectivity corrections of the crystal to the line intensities. The theoretical linewidths have been adjusted to correspond to the experimental linewidths, and $f_\perp/f_\parallel$ was taken to be 0.125.

have been corrected for polarization and for crystal reflectivity as described in the next section. Each of the *KLL* satellite lines in the spectrum of Fig. 4(a) has been fitted to a Gaussian profile using a least-squares technique, the resulting central channel numbers have been converted to wavelengths using the DE calibration described above. The measured wavelengths are shown in Table I along with the theoretical wavelengths for these lines. The Auger energies, x-ray energies, and the 4π-averaged resonance strengths for the heliumlike lines, shown in Fig. 4(b) and Table I, have been obtained from the Hebrew University-Lawrence Livermore Atomic Code (HULLAC) package, which calculates wave functions, energy levels, and radiative transition rates by the relativistic, multiconfiguration parametric potential method with full configuration interaction [18]. Also shown in Table I and used to plot Fig. 4(c) are heliumlike atomic-structure parameters from Vainshtein and Safronova [19]. These were calculated with a $1/Z$ expansion perturbation technique with relativistic corrections taken into account within the framework of the Breit operator.

Similar theoretical and experimental data for the berylliumlike lines are shown in Table II; the lines have been labeled with numbers according to their uncorrected line strengths. The Auger and x-ray energies were calculated using the multiconfiguration Dirac-Fock (MCDF) model including Breit and QED corrections [20]. The 4π-averaged DR resonance strengths and the linear polarization fractions were computed from perturbation theory using the MCDF method [21].

There is, in general, agreement between the measured and the various theoretical wavelengths shown in Tables I and II. The Li-like lines *u* and *l* and several of the Be-like lines with identification numbers 10 and above have low intensities and rather large uncertainties ($\geq 0.000\,15$ Å) associated with their observed wavelengths. These lines appear to be blended with other low-intensity lines and we have not been able to obtain the resonance strengths of these lines by the technique described below.

The DR resonances are narrow ($\leq$ FWHM 0.5 eV) compared to the electron beam, which has a Gaussian energy distribution with FWHM 50 eV. Thus, as the electron-beam energy is swept through the resonances, each DR line makes a larger or smaller contribution to the spectrum depending on how much of the electron beam samples the resonance. We have obtained the intensity of each satellite line as a function of excitation energy and fitted each curve to a Gaussian profile. In Fig. 5(a), the intensity of the line *j* is shown. The curve has a FWHM of 50 eV, corresponding to the spread of the electron beam. In Fig. 5(b) is shown the combined intensity curves for the lines *t* and *m*; these lines are clearly resolved in Fig. 5(b) since their resonance energies, 4998 and 5069 eV, respectively, are separated by more than the electron-beam energy spread. The lines *t* and *m* have wavelengths 1.7180 and 1.7177 Å, respectively; they could not be resolved by our spectrometer and appear blended in Fig. 4(a). We have integrated the intensity functions for all the prominent *KLL* lines and used these to calculate the resonance line strengths. The line

TABLE I. Satellite transitions of lithiumlike cobalt labeled according to a notation by Gabriel [16]. The theoretical wavelengths, resonance strengths (S), and Auger energies (E_{au}) are from atomic-structure calculations: (a) present work and (b) by Vainshtein and Safronova [19]. Polarizations (P) are from Inal and Dubau [26]. $G[s,j]$ is the crystal response factor for each line relative to that of j [see Eq. (8) in the text]. Resonance strengths are expressed in units of 10^{-20} cm^2 eV.

Key	Transitions	E_{au} (eV)	λ (Å)[a]	λ (Å)[b]	λ (Å)[expt]	P	$G[s,j]$	S^a	S^b
a	$(1s2p_{3/2}^2)_{3/2}\rightarrow 1s\,^2 2p_{3/2}$	5049.30	1.7224	1.7225	1.722 37(0.000 08)	−0.8	0.196	1.118	1.439
b	$(1s2p_{1/2}^2)_{3/2}\rightarrow 1s^2 2p_{1/2}$	5049.30	1.7180	1.7181		0.6	1.110	0.100	0.100
c	$(1s2p_{1/2}2p_{3/2})_{1/2}\rightarrow 1s\,^2 2p_{3/2}$	5028.17	1.7275	1.7275		0.0	0.609	0.014	0.013
d	$(1s2p_{1/2}2p_{3/2})_{1/2}\rightarrow 1s\,^2 2p_{1/2}$	5028.17	1.7230	1.7231		0.0	0.609	0.048	0.045
e	$(1s2p_{1/2}2p_{3/2})_{5/2}\rightarrow 1s\,^2 2p_{3/2}$	5007.86	1.7324	1.7322	1.732 35(0.000 12)	0.5	1.000	4.555	5.733
f	$(1s2p_{1/2}2p_{3/2})_{3/2}\rightarrow 1s\,^2 2p_{3/2}$	4999.47	1.7344	1.7338		−0.8	0.196	0.048	0.038
g	$(1s2p_{1/2}2p_{3/2})_{3/2}\rightarrow 1s\,^2 2p_{1/2}$	4999.47	1.7299	1.7293		0.6	1.110	0.005	0.001
h	$(1s2p_{1/2}^2)_{1/2}\rightarrow 1s\,^2 2p_{3/2}$			1.7362		0.0	0.609		
i	$(1s2p_{1/2}^2)_{1/2}\rightarrow 1s\,^2 2p_{1/2}$	4989.83	1.7322	1.7316		0.0	0.609	0.028	0.026
j	$(1s2p_{3/2}^2)_{5/2}\rightarrow 1s\,^2 2p_{3/2}$	5035.38	1.7257	1.7259	1.725 94(0.000 07)	0.5	1.000	25.429	28.017
k	$(1s2p_{1/2}2p_{3/2})_{3/2}\rightarrow 1s\,^2 2p_{1/2}$	5026.47	1.7234	1.7232	1.723 26(0.000 06)	0.6	1.110	17.355	20.420
l	$(1s2p_{1/2}2p_{3/2})_{3/2}\rightarrow 1s\,^2 2p_{3/2}$	5026.47	1.7279	1.7277	1.727 86(0.000 17)	−0.8	0.196	0.341	0.448
m	$(1s2p_{3/2}^2)_{1/2}\rightarrow 1s\,^2 2p_{3/2}$	5069.30	1.7176	1.7177	1.717 91(0.000 07)	0.0	0.609	1.371	1.690
n	$(1s2p_{3/2}^2)_{1/2}\rightarrow 1s\,^2 2p_{1/2}$	5069.30	1.7132	1.7134		0.0	0.609	0.042	0.059
o	$(1s2s^2)_{1/2}\rightarrow 1s\,^2 2p_{3/2}$	4916.92	1.7547	1.7544		0.0	0.609	0.512	0.507
p	$(1s2s^2)_{1/2}\rightarrow 1s\,^2 2p_{1/2}$	4916.92	1.7501	1.7499		0.0	0.609	0.523	0.550
q	$(1s2s2p_{3/2})_{3/2}\rightarrow 1s\,^2 2s_{1/2}$	4983.92	1.7213	1.7215	1.721 26(0.000 11)	0.6	1.110	0.064	0.137
r	$(1s2s2p_{1/2})_{1/2}\rightarrow 1s\,^2 2s_{1/2}$	4971.33	1.7242	1.7241	1.724 26(0.000 08)	0.0	0.609	2.355	1.906
s	$(1s2s2p_{3/2})_{3/2}\rightarrow 1s\,^2 2s_{1/2}$	5001.44	1.7170	1.7172		0.6	1.110	0.828	0.033
t	$(1s2s2p_{3/2})_{1/2}\rightarrow 1s\,^2 2s_{1/2}$	4998.09	1.7178	1.7180	1.717 91(0.000 07)	0.0	0.609	3.206	3.714
u	$(1s2s2p_{1/2})_{3/2}\rightarrow 1s\,^2 2s_{1/2}$	4933.88	1.7333	1.7332	1.733 61(0.000 18)	0.6	1.110	0.387	0.214
v	$(1s2s2p_{1/2})_{1/2}\rightarrow 1s\,^2 2s_{1/2}$	4928.27	1.7346	1.7342		0.0	0.609	0.055	0.017

[a]Present calculations.
[b]See Vainshtein and Safronova, Ref. [19].

TABLE II. Berylliumlike satellite transitions to the $K\alpha$ lines of heliumlike cobalt. Transitions have been labeled with numbers corresponding to the uncorrected strength of the transition. The parameters wavelength, polarization, and Auger energies are from present MCDF calculations. $G[s,j]$ is the crystal response factor for each line relative to that of j [see Eq. (8) in the text]. Resonance strengths are expressed in units of 10^{-20} cm^{2}eV.

Key	Transitions	E_{au} (eV)	λ_{Theor} (Å)	λ_{Expt} (Å)	P	$G[s/j]$	S
1	$(1s2s2p_{3/2}^2)_3\rightarrow(1s\,^2 2s2p_{3/2})_2$	5090.69	1.734 64	1.734 81(0.00008)	0.439	0.944	14.13
2	$(1s2s2p_{1/2}2p_{3/2})_2\rightarrow(1s\,^2 2s2p_{1/2})_1$	5084.68	1.732 79	1.732 82(0.00009)	0.337	0.856	7.883
3	$(1s2s2p_{1/2}2p_{3/2})_2\rightarrow(1s\,^2 2s2p_{3/2})_2$	5095.50	1.733 47	1.733 61(0.00018)	−0.577	0.293	5.305
4	$(1s2s2p_{1/2}2p_{3/2})_1\rightarrow(1s\,^2 2s2p_{1/2})_1$	5090.30	1.731 43	1.731 47(0.00011)	−0.428	0.364	4.209
5	$(1s2s2p_{1/2}2p_{3/2})_2\rightarrow(1s\,^2 2s2p_{3/2})_1$	5116.02	1.737 61	1.736 91(0.00011)	0.587	1.085	4.005
6	$(1s2s2p_{1/2}2p_{3/2})_2\rightarrow(1s\,^2 2s2p_{3/2})_2$	5116.02	1.728 51	1.729 12(0.00011)	−0.965	0.132	2.721
7	$(1s2s2p_{1/2}2p_{3/2})_2\rightarrow(1s\,^2 2s2p_{3/2})_2$	5084.68	1.736 10		−0.435	0.361	1.390
8	$(1s2s2p_{1/2}2p_{3/2})_1\rightarrow(1s\,^2 2s2p_{3/2})_2$	5124.15	1.726 66	1.726 72(0.00017)	0.202	0.750	1.289
9	$(1s2s2p_{3/2}^2)_2\rightarrow(1s\,^2 2s2p_{3/2})_1$	5129.84	1.734 25		0.587	1.085	0.951
10	$(1s2s\,^2 2p_{1/2})_1\rightarrow(1s\,^2 2s^2)_0$	5009.73	1.738 95	1.737 78(0.00022)	−0.972	0.129	0.886
11	$(1s2s2p_{1/s}2p_{3/2})_1\rightarrow(1s\,^2 2s2p_{1/2})_0$	5080.03	1.732 85		0.515	1.014	0.882
12	$(1s2s2p_{1/2}2p_{3/2})_3\rightarrow(1s\,^2 2s2p_{3/2})_2$	5046.87	1.745 34	1.745 4(0.00015)	0.439	0.944	0.798
13	$(1s2s2p_{3/2}^2)_0\rightarrow(1s\,^2 2s2p_{3/2})_1$	5146.21	1.730 27		0	0.608	0.704
14	$(1s2s2p_{1/2}2p_{3/2})_1\rightarrow(1s\,^2 2s2p_{1/2})_0$	5090.30	1.730 37	1.730 79(0.00015)	0.600	1.098	0.686
15	$(1s2s2p_{1/2}2p_{3/2})_1\rightarrow(1s\,^2 2s2p_{3/2})_2$	5090.30	1.734 73		0.731	1.239	0.651
16	$(1s2s2p_{1/2}2p_{3/2})_1\rightarrow(1s\,^2 2s2p_{3/2})_2$	5106.33	1.730 85	1.730 79(0.00015)	0.142	0.706	0.501
17	$(1s2s2p_{1/2}2p_{3/2})_1\rightarrow(1s\,^2 2s2p_{1/2})_1$	5106.33	1.727 56	1.727 15(0.00017)	−0.710	0.234	0.489
18	$(1s2s2p_{1/2}2p_{3/2})_1\rightarrow(1s\,^2 2s2p_{3/2})_2$	5080.03	1.737 23		0.609	1.107	0.320
19	$(1s2s2p_{1/2}2p_{3/2})_1\rightarrow(1s\,^2 2s2p_{3/2})_1$	5106.33	1.739 97		−0.710	0.234	0.293
20	$(1s2s2p_{1/2}2p_{3/2})_2\rightarrow(1s\,^2 2s2p_{3/2})_1$	5095.50	1.742 62	1.743 31(0.00022)	0.417	0.925	0.276
21	$(1s2s2p_{1/2}2p_{3/2})_1\rightarrow(1s\,^2 2s2p_{1/2})_1$	5080.03	1.733 92		−0.347	0.406	0.268

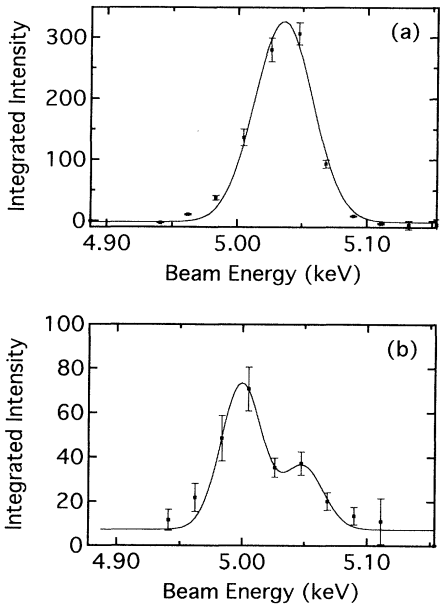

FIG. 5. Variation of intensity of the dielectronic resonance lines with excitation energy. The lines have been fitted with a Gaussian profile, which has a FWHM of 50 eV, corresponding to the width of the electron beam. Shown in (a) are the excitation function of the line *j*; in (b) the excitation function of the lines *t* and *m*; these overlap in wavelength but have resonance energies which differ by 71 eV and are clearly resolved in this figure.

strengths are then corrected for polarization and crystal reflectivity, as discussed in detail below, and the results are shown in Table III.

IV. THEORY

A. Relative dielectronic resonance strengths

In the following, we follow the procedure described in Ref. [13] for determining the resonance strength from the intensity functions of each satellite line measured. The resonance strength can be defined as

$$S_s = \int_{-\infty}^{\infty} \sigma(E - E_{\rm au}) dE \ , \tag{3}$$

where $\sigma(E-E_{\rm au})$ is the excitation cross section for electrons with energy E; $E_{\rm au}$ is the resonance energy. This may be shown to be given by

$$S_s = F_2 \frac{1}{E_{\rm au}} 2\pi^2 a_0^3 R^2 \left[\frac{m_e}{2R}\right]^{1/2} , \tag{4}$$

where a_0, m_e, and R are the Bohr radius, the mass of the electron, and the Rydberg energy, respectively, and F_2 is the satellite-specific line factor given by

$$F_2 = \frac{g_s}{g_i} \frac{A_a^{si} A_r^{sf}}{\Sigma_j A_a^{sj} + \Sigma_{f'} A_r^{sf'}} \ . \tag{5}$$

TABLE III. Relative resonance strengths of lithiumlike and berylliumlike DR satellite lines of cobalt. The line strengths are shown relative to the strength of *j* for lithiumlike lines, and to the strength of 1 for berylliumlike lines. The theoretical values are from present calculations (S^a) and from calculations by Vainshtein and Safronova (S^b) [19]. The experimental line strengths have been corrected for crystal response. Resonance strengths are expressed in units of 10^{-20} cm^2 eV.

Key	$S^{\rm Expt}$	S^a	S^b
a	49.8(3.2)	24.5	28.7
e	20.7(3.1)	17.9	20.5
j	100.0(4.3)	100.0	100.0
k	67.0(5.2)	68.1	66.3
m	7.4(2.5)	9.0	10.1
r	22.9(6.4)	15.4	11.3
t	25.5(4.0)	21.0	22.1
1	100.0(3.4)	100.0	
2	66.9(3.7)	55.8	
3	35.3(7.1)	37.6	
4	37.5(7.1)	29.8	
5	26.9(2.4)	28.4	
6	42.0(7.1)	19.2	
9	36.2(3.8)	9.8	

[a]Relative S values based on present calculations.
[b]Relative S values based on calculations by Vainshtein and Safronova, Ref. [19].

Here A_a^{si} is the autoionization rate from the upper level $|s\rangle$ to the ground state $|i\rangle$ of the recombining ion, and A_r^{sf} is the radiative decay rate from upper level $|s\rangle$ to lower level $|f\rangle$; g_s and g_i are the statistical weights of the autoionizing and the recombining ground states, respectively. Evaluating the constants in Eq. (5) above gives

$$S_s = 2.475\times10^{-30}[F_2(\sec^{-1})]/[E_{\rm au}({\rm eV})]{\rm cm}^2\,{\rm eV} \ . \tag{6}$$

In terms of the resonance strength and the electron energy distribution at the resonance energy $f(E_{\rm au}-E_0)$, the satellite intensity may be written as

$$I_s(E_0) = \frac{j}{e} f(E_{\rm au}-E_0) n_{\rm He} S_s \ , \tag{7}$$

where j is the electron current density and $n_{\rm He}$ is the density of ions in the heliumlike (lithiumlike) charge state. In this experiment, we have measured the energy excitation function for each of the more prominent *KLL* transitions, integrated each function to obtain the experimental resonance strength, and then normalized these measured values to that for the most intense satellite *j*. In the resulting ratio, the dependence of the resonance strengths on the beam current density and the density of ions in the heliumlike charge state drop out and we have

$$S_s = S_j \frac{\int_{-\infty}^{+\infty} I_s dE_0}{\int_{-\infty}^{+\infty} I_j dE_0} \ . \tag{8}$$

Similar equations can be written down for berylliumlike satellites, in which $n_{\rm He}$ is replaced by $n_{\rm Li}$ in Eq. (7), and S_j and I_j, are replaced by S_1 and I_1 in Eq. (8), respectively. ($n_{\rm Li}$ is the density of lithiumlike ions, and S_1 and I_1

are the resonance strength and intensity of the strongest Be-like satellite.) Equation (8) allows us to calculate uncorrected dielectronic resonance strengths of each of the observed satellite lines relative to that of the line j or line 1. In Sec. IV B we discuss how these ratios may be corrected for polarization and anisotropy of the emitted x rays.

B. Polarization correction

The radiation from EBIT is polarized and anisotropic [22]. In EBIT, the direction of the electron beam establishes a preferred direction in space; the intensity of x rays emitted at 90° to the beam $I(90°)$ is different from the 4π-averaged value $\langle I \rangle$. For electric dipole transitions, the emission perpendicular to the beam and the space-averaged value are related by

$$I(90°)=\frac{3}{3-P}\langle I \rangle , \tag{9}$$

where P is the linear polarization. If $I_{\parallel}$ and $I_{\perp}$ are the intensities of radiation with the electric-field vector parallel and perpendicular to the electron beam, respectively, then P is defined as

$$P=\frac{I_{\parallel}-I_{\perp}}{I_{\parallel}+I_{\perp}} . \tag{10}$$

The denominator in the latter equation is just the quantity $I(90°)$.

The crystal preferentially reflects x rays, which have their electric fields parallel to the electron beam, so that the observed intensity $I^{\rm obs}$ is different from $I(90°)$. If $f_{\parallel}$ and $f_{\perp}$ are the crystal reflectivities for x rays polarized parallel and perpendicular to the beam, then $I^{\rm obs}$ is given by

$$I^{\rm obs}=f_{\parallel}I_{\parallel}+f_{\perp}I_{\perp} . \tag{11}$$

Similar to a procedure used in Ref. [13], we define a relative crystal response function G, which relates an observed intensity ratio to the 4π-averaged value (the value most likely to be calculated from theory); thus,

$$\frac{I_s^{\rm obs}}{I_j^{\rm obs}}=G[s,j]\frac{\langle I_s \rangle}{\langle I_j \rangle} . \tag{12}$$

The factor G, which takes into account the anisotropy of the emitted beam and the differential reflectivity of the crystal, is given by

$$G[s,j]\equiv\frac{f_{\parallel}^{s}(1+P_s)+f_{\perp}^{s}(1-P_s)3-P_j}{f_{\parallel}^{j}(1+P_j)+f_{\perp}^{j}(1-P_j)3-p_s} . \tag{13}$$

Each measured resonance strength from Eq. (8) above is divided by G from Eq. (13) and this corrected value is compared with theory. For these measurements, which were carried out with a quartz crystal, and for which the central Bragg angle is 38.7°, the ratio $f_{\perp}/f_{\parallel}$ is expected to have a value between 0.218 and 0.048, values that correspond to the case of an ideal or of a mosaic crystal, respectively [23]. In our analysis of the relative line intensities we used $f_{\perp}/f_{\parallel}=0.125$, which is the average value for an ideal and mosaic crystal at the Bragg angles of interest. This value is close to the value $f_{\perp}/f_{\parallel}=0.15$ calculated by Hölzer and Förster [24] using the dynamical theory for a perfect crystal following the treatment of the integrated crystal reflectivities given by Taupin [25].

We present in Fig. 6 three synthetic spectra that show the effect of correction for polarization and crystal reflectivity on calculated line intensities. In Fig. 6(a), the isotropic line intensities are shown as determined by atomic parameters listed in Tables I and II. The anistropy of x-ray lines for emission at 90° to the electron beam and the reflectivity of the crystal have been taken into account in Figs. 6(b) and 6(c). The ratio of crystal reflectivities $f_{\perp}/f_{\parallel}=0.125$ and 0.218 were used in Figs. 6(b) and 6(c), respectively. There is a marked difference between the isotropic line intensities of Fig. 6(a) and those to which corrections have been applied in Figs. 6(b) and 6(c). The lithiumlike satellite lines a, r, and l, and the Be-like satellite lines 6, 4, and 3 are more prominent in Fig. 6(a) than in 6(b) and 6(c). There is, however, very little difference between 6(b) and 6(c). It should be noted further that only the corrected Figs. 6(b) and 6(c) are representative of the measured spectrum shown in Fig. 4(a). These findings clearly show that the corrections for polarization and crystal reflectivity are important, but that the correction is not very sensitive to the value of $f_{\perp}/f_{\parallel}$ used.

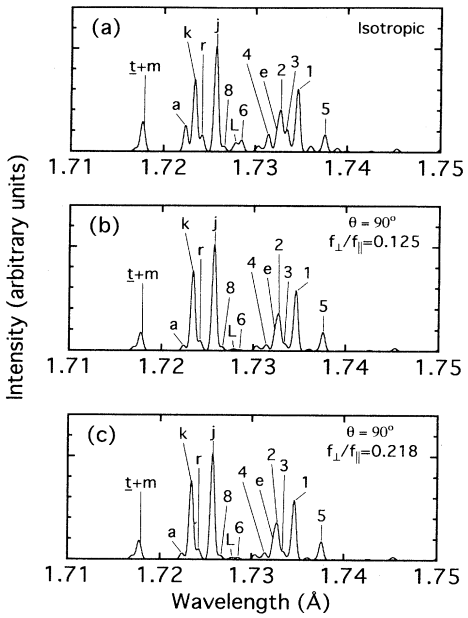

FIG. 6. Theoretical line intensities showing the effect of correction for line polarization and for crystal reflectivity. (a) shows the isotropic intensities, as they are normally calculated in theory. The intensities shown in (b) and (c) have been corrected for emission at 90° to the electron beam, and for crystal reflectivities assuming $f_{\perp}/f_{\parallel}=0.125$ and 0.218, respectively. (b) and (c) are similar to each other and to the experimental spectrum, but quite different from (a). This indicates that the corrections are necessary, but relatively insensitive to the value of the ratio of crystal reflectivities.

V. DISCUSSION

There is, in general, agreement between predicted and observed resonance strengths, as can be seen in both Fig. 4 and Table III. In Fig. 4, the general features of the experimental spectrum are clearly reproduced by theory, provided the theory is corrected for polarization and crystal reflectivities. A closer look at the data, however, reveals some discrepancies. The data in Table II show that our theoretical calculations and those of Ref. [19] underestimate the resonance strengths of line *a* by 51% and 42%, respectively, and of line *r* by 33% and 51%, respectively. The latter finding is consistent with the result obtained in Ref. [13] for line *r* in iron. Table III also shows that both theories also tend to overestimate the strength of line *m* (this was also the case in Ref. [13]). Here, as well as in Ref. [13], we note that there is better agreement between theory and the experiment for the strongest lithiumlike lines *k*, *e*, and *t*, as well as for the strongest berylliumlike lines 2–5. The worst case disagreement between theory and experiment is associated with lines that have negative polarizations, line *a* with $P=-0.8$ and line 6 with $P=-0.946$. Although there is good overall agreement between experiment and theory, these results and those of Ref. [13] clearly indicate that particular details of the satellite spectrum of heliumlike ions are not yet completely understood and require additional attention in order to bring theory and experiment closer together.

ACKNOWLEDGMENTS

We gratefully acknowledge G. Hölzer and E. Förster of the Max-Planck-Arbeitsgruppe "Röntgenoptik" at the Friedrich-Schiller University, Jena, Germany for calculation of the $f_{\perp}/f_{\parallel}$ factor for quartz. We also gratefully acknowledge K. J. Reed and the Lawrence Livermore National Laboratory Research Collaborations Program for Historically Black Colleges and Universities. This work was performed under a Department of Energy Contract No. W-7405-ENG-48 at the Lawrence Livermore National Laboratory.

[1] K. W. Hill, S. von Goeler, M. Bitter, L. Campbell, R. D. Cowan, B. Fraenkel, A. Greenberger, R. Horton, J. Hovey, W. Roney, N. R. Sauthoff, and W. Stodiek, Phys. Rev. A **19**, 1770 (1979).

[2] M. Bitter, S. von Goeler, M. Goldman, K. W. Hill, R. Horton, W. Roney, N. Sauthoff, and W. Stodiek, in *Temperature, its Measurement and Control in Science and Industry,* edited by S. F. Schooley (American Institute of Physics, New York, 1992), Vol. 5, p. 693.

[3] J. F. Seely, U. Feldman, and U. I. Safronova, Astrophys. J. **304**, 838 (1986).

[4] F. Bely-Dubeau, A. H. Gabriel, and S. Volonte, Mon. Not. R. Astron. Soc. **189**, 801 (1949).

[5] H. Hsuan, M. Bitter, J. E. Rice, K. W. Hill, L. Johnson, S. L. Liew, S. D. Scott, and S. von Goeler, Rev. Sci. Instrum. **59**, 2127 (1988).

[6] M. Bitter, K. W. Hill, N. R. Sauthoff, P. C. Efthimion, E. Merservey, W. Roney, S. von Goeler, R. Horton, M. Goldman, and W. Stodiek, Phys. Rev. Lett. **43**, 129 (1979).

[7] TFR Group, J. Dubau, and M. Loulergue, J. Phys. B **15**, 1007 (1982).

[8] M. Bitter, H. Hsuan, J. E. Rice, K. W. Hill, M. Diesso, B. Grek, R. Hulse, D. W. Johnson, L. C. Johnson, and S. von Goeler, Rev. Sci. Instrum. **59**, 2131 (1988).

[9] M. A. Levine, R. E. Marrs, J. R. Henderson, D. A. Knapp, and M. B. Schneider, Phys. Scr. **T22**, 157 (1988).

[10] R. E. Marrs, M. A. Levine, D. A. Knapp, and J. R. Henderson, Phys. Rev. Lett. **60**, 1715 (1988).

[11] D. A. Knapp, R. E. Marrs, M. A. Levine, C. L. Bennett, M. H. Chen, J. R. Henderson, M. B. Schneider, and J. H. Scofield, Phys. Rev. Lett. **62**, 2104 (1989).

[12] P. Beiersdorfer, M. H. Chen, R. E. Marrs, M. B. Schneider, and R. S. Walling, Phys. Rev. A **44**, 396 (1991).

[13] P. Beiersdorfer, T. W. Phillips, K. L. Wong, R. E. Marrs, and D. A. Vogel, Phys. Rev. A **46**, 3812 (1992).

[14] P. Beiersdorfer, R. E. Marrs, J. R. Henderson, D. A. Knapp, M. A. Levine, D. B. Platt, M. B. Schneider, D. A. Vogel, and K. L. Wong, Rev. Sci. Instrum. **61**, 2338 (1990).

[15] P. Beiersdorfer, V. Decaux, S. R. Elliot, K. Widmann, and K. Wong, Rev. Sci. Instrum. **66**, 303 (1995).

[16] A. H. Gabriel, Mon. Not. R. Astron. Soc. **160**, 99 (1972).

[17] G. W. Drake, Can. J. Phys. **66**, 586 (1988).

[18] M. Klapisch, Comput. Phys. Commun. **2**, 239 (1971); M. Klapish, J. L. Schwob, B. S. Fraenkel, and J. Oreg, J. Opt. Soc. Am. **61**, 148 (1977).

[19] L. A. Vainshtein and U. I. Safronova, At. Data Nucl. Data Tables **25**, 49 (1978).

[20] I. P. Grant, B. J. Mckenzie, P. H. Norrington, D. F. Mayers, and N. C. Pyper, Comput. Phys. Commun. **21**, 207 (1980).

[21] M. H. Chen, in *Recombination of Atomic Ions,* Vol. 296 of *NATO Advanced Study Institute, Series B: Physics,* edited by W. G. Graham, W. Fritsch, Y. Hahn, and J. A. Tanis (Plenum, New York, 1992), p. 61.

[22] D. A. Vogel, Ph.D thesis, Georgia Institute of Technology, 1992.

[23] A. Burek, Space Sci. Instrum. **2**, 53 (1976).

[24] G. Hölzer and E. Förster (private communication).

[25] D. Taupin, Bull. Soc. Fr. Mineral Cristallog. **87**, 469 (1964).

[26] M. K. Inal and J. Dubau, J. Phys. B **22**, 3329 (1989).